Chap. VII. Nuclear Reactions — The Optical Model

Ref: Foderaro, Chap. 7
Feshbach, Porter, Weisskopf, Phys. Rev. 96, 448 (1954)
P. E. Hodgson, Optical Model of Elastic Scattering (Oxford, 1963).

As an application of the method of partial waves we will study the optical model as used in the calculation of nuclear cross sections. The basic idea here is to postulate a complex potential for the interaction between an incident particle, such as a neutron or a proton, and the target nucleus. The potential is meant to be a very crude approximation to the actual nuclear interactions, so the motivation of the calculation is not to try to describe any of the fine details of nuclear reactions, such as an individual resonance reaction; instead one is looking for a simple method of estimating the cross section that can be used for any nucleus and over a wide range of energy.

We recall from Chap. VI that the cross section can be expressed in terms of the quantity $\eta_\ell = \exp(2i\delta_\ell)$. When the optical model is used to calculate η_ℓ, the result is to be regarded as an approximation to an energy averaged quantity $\langle\eta_\ell\rangle$, with $\langle\ \rangle$ denoting an average over a certain energy interval such that all sharp resonances are smoothed over. In other words, in the present approach one can only expect to obtain the gross behavior of cross section variations with energy and with mass number A. If one were interested in the details of resonance behavior, then one should consider the Breit-Wigner resonance cross section formalism which can be extended to treat multichannel, multilevel reactions.

A. Cross Section for Reaction

We have thus far discussed interaction potentials V(r) which are real. With V(r) real the only interaction process possible is elastic scattering. In order to describe reaction interactions one can assume a complex potential, the simplest example of wich is the square well,

$$V(r) = \begin{cases} -V_o - iW_o & r < r_o \\ 0 & r > r_o \end{cases} \tag{7.1}$$

For typical values one can take $V_o = 42$ MeV, $W_o/V_o = 0.03$, and $r_o = 1.45A^{1/3} \times 10^{-13}$ cm. The presence of an imaginary part in V(r) means that the phase shift δ_ℓ now becomes complex. If we write

$$\eta_\ell \equiv e^{2i\delta_\ell} \longrightarrow e^{2i(\delta_\ell + i\gamma_\ell)} \tag{7.2}$$

with η_ℓ now denoting the real part of the phase shift and γ_ℓ the imaginary part, then clearly $|\eta_\ell| = \exp(-2\gamma_\ell)$. The fact that the magnitude of $|\eta_\ell|$ is no longer unity implies that the 'scattering' process can result in a reaction. Depending on the sign of γ_ℓ the reaction can be an absorption or a creation process. Given this simple modification the cross section results (6.22) and (6.23) can be written as

$$\sigma_{el}(\theta) = (\lambda\!\!\!^{-2}/4)\left|\sum_{\ell=0}^{\infty}(2\ell+1)(\eta_\ell - 1)\,P_\ell(\cos\theta)\right|^2 \tag{7.3}$$

$$\boxed{\sigma_{el} = \pi\lambda\!\!\!^{-2}\sum_{\ell=0}^{\infty}(2\ell+1)\,|1-\eta_\ell|^2} \tag{7.4}$$

We have added the subscript to indicate that (6.22) is only the elastic scattering part of the cross section. (In the terminology of nuclear reactions elastic scattering is not considered a true reaction process, it is sometimes called an improper reaction.)

To find the reaction part of the cross section we adopt the definition of the reaction cross section,

$$\sigma_r \equiv (1/I_o)[J^R_{in} - J^R_{out}] \tag{7.5}$$

where $I_o = \hbar k/\mu$ is the unit incident flux, and J^R is the radial component of the current vector $\underline{J}$, with subcripts denoting incident and outgoing (previously we had used the term 'scattered') components. By the radial currents we mean operationally,

$$J^R = r^2 \int d\Omega\, \hat{\underline{r}} \cdot \underline{J} \tag{7.6}$$

the integral being over the surface of a large sphere of radius r. In (7.5) the current $\underline{J}$ can be calculated from (6.3) once the wave function is known. From (6.16) and (6.20) we can write the total wave function in the asymptotic region as

$$\psi(r,\theta) = \sum_\ell \frac{i^\ell(2\ell+1)\,P_\ell}{2ikr}\left[\eta_\ell e^{i(kr-\ell\pi/2)} - e^{-i(kr-\ell\pi/2)}\right]$$

$$= \psi_{out} + \psi_{in} \tag{7.7}$$

Having identified the two wave functions we can find the corresponding currents from (6.3) and the radial currents from (7.6). The resulting expression for the reaction cross section is

$$\sigma_r(k) = \pi\lambda\!\!\!^{-2} \sum_\ell (2\ell+1)\ [1 - |\eta_\ell|^2] \tag{7.8}$$

We can define the total cross section σ_t as the sum of σ_{el} and σ_r,

$$\sigma_t(k) = 2\pi\lambda\!\!\!^{-2} \sum_\ell (2\ell+1)\ [1 - \mathrm{Re}\{\eta_\ell(k)\}] \tag{7.9}$$

One now must remember that η_ℓ is complex.

B. Energy Averaging

As we have already mentioned, the scattering amplitude η^{opt} calculated using the optical model potential is meant to be an approximation to the energy averaged η which we will denote as

$$\langle\eta\rangle \equiv \Delta^{-1} \int_{E-\Delta/2}^{E+\Delta/2} dE'\ \eta(E') \tag{7.10}$$

Applying this averaging procedure to σ_{el} and σ_r, we obtain

$$\langle\sigma_{el}\rangle = \pi\lambda\!\!\!^{-2} \sum (2\ell+1)\ [|1 - \langle\eta_\ell\rangle|^2 + \langle|\eta_\ell|^2\rangle - |\langle\eta_\ell\rangle|^2]$$

$$= \sigma_{se} + \sigma_{ce} \tag{7.11}$$

$$\langle\sigma_r\rangle = \pi\lambda\!\!\!^{-2} \sum_\ell (2\ell+1)\ [1 - \langle|\eta_\ell|^2\rangle] \tag{7.12}$$

In (7.11) we have decomposed the elastic scattering cross section into two components, the shape elastic scattering cross section σ_{se} and the compound elastic cross section σ_{ce}, the latter being made out of the second and third terms in the bracket in (7.11).

One should notice that from the optical model we get $\langle\eta_\ell\rangle$ and therefore $|\langle\eta_\ell\rangle|^2$, but we do not know $\langle|\eta_\ell|^2\rangle$. This means the optical model cannot give $\langle\sigma_r\rangle$ or σ_{ce}. On the other hand we can calculate the sum of $\langle\sigma_r\rangle$ and σ_{ce}, a quantity we will call the compound formation cross section,

$$\sigma_c \equiv \langle\sigma_r\rangle + \sigma_{ce} = \pi\lambda\!\!\!^{-2} \sum (2\ell+1)\ [1 - |\langle\eta_\ell\rangle|^2] \tag{7.13}$$

Summarizing our results we see that once $\langle\eta_\ell\rangle$ is known, we can obtain the shape elastic cross section as

$$\boxed{\sigma_{se} = \pi\lambda\!\!\!^{-2} \sum_\ell (2\ell+1)\ |1 - \langle\eta_\ell\rangle|^2} \tag{7.14}$$

the compound formation cross section from (7.13), and the total cross section $\sigma_t = \sigma_{se} + \sigma_c$ from (7.9) with η_ℓ replaced by $\langle\eta_\ell\rangle$.

A similar decomposition can be carried out for the angular differential cross section for elastic scattering. Thus we rewrite (7.3) as

$$\langle\sigma_{el}(\theta)\rangle = \langle\sigma_{se}(\theta)\rangle + \langle\sigma_{ce}(\theta)\rangle \tag{7.14}$$

with

$$\langle\sigma_{se}(\theta)\rangle = (\lambda\!\!\!^{-2}/4)\ \left|\sum (2\ell+1)(1 - \langle\eta_\ell\rangle)P_\ell(\cos\theta)\right|^2 \tag{7.15}$$

and

$$\langle\sigma_{ce}(\theta)\rangle = (\lambda\!\!\!^{-2}/4)\sum_\ell (2\ell+1)(2\ell'+1)P_\ell(\cos\theta)P_{\ell'}(\cos\theta)\,[\langle\eta^*_\ell\eta_{\ell'}\rangle - \langle\eta^*_\ell\rangle\langle\eta_{\ell'}\rangle] \tag{7.16}$$

It is again clear from (7.15) and (7.16) why the optical model is able to give $\langle\sigma_{se}(\theta)\rangle$ but not $\langle\sigma_{ce}(\theta)\rangle$.

If one has no further information about the phase shifts one could simplify the calculation somewhat by assuming there is no interference between states of different angular momentum. By inserting

$$\langle\eta^*_\ell\eta_{\ell'}\rangle - \langle\eta^*_\ell\rangle\langle\eta_{\ell'}\rangle \simeq [\langle|\eta_\ell|^2\rangle - |\langle\eta_\ell\rangle|^2]\ \delta_{\ell\ell'} \tag{7.17}$$

into (7.16) one obtains

$$\langle\sigma_{ce}(\theta)\rangle \simeq \frac{1}{4}\sum_\ell (2\ell+1)\ \sigma^{(\ell)}_{el}(k)\ P^2_\ell(\cos\theta) \tag{7.18}$$

with

$$\sigma^{(\ell)}_{el}(k) = \lambda\!\!\!^{-2}(2\ell+1)[\langle|\eta_\ell|^2\rangle - |\langle\eta_\ell\rangle|^2] \tag{7.19}$$

The assumption of no interference thus reduces the calculation of the differential cross section to the same level as that of the total (in the

sense of integration over scattering angle) cross section. Still, without further approximation one cannot calculate $\langle\sigma_{ce}(\theta)\rangle$. The quantity that is not given by the optical model is the first term in the bracket in (7.19). Suppose we replace $\langle|\eta_\ell|^2\rangle$ by unity, then in most cases this would amount to an upper estimate of $\langle|\eta_\ell|^2\rangle$ since with the exception of fission reaction the imaginary part of the phase shift γ_ℓ (cf. (7.2)) is usually positive. The approximation therefore corresponds to writing the compound formation cross section (7.13) as

$$\sigma_c = \pi \sum_\ell \sigma_c^{(\ell)} \tag{7.20}$$

where

$$\sigma_c^{(\ell)} = \lambda\!\!\!^{-2}(2\ell+1)[1 - |\langle\eta_\ell\rangle|^2] \tag{7.21}$$

and replacing in (7.18) $\sigma_{el}^{(\ell)}$ by $\sigma_c^{(\ell)}$. One expects that this will provide an upper bound on $\langle\sigma_{ce}(\theta)\rangle$.

C. Square Well Potential

The simplest calculation of η_ℓ^{opt} is to apply the result (6.33) to the square well potential (7.1). It turns out that recurrence relations can be derived for q_ℓ^{int} and $q_\ell^{(\pm)}$ which can greatly facilitate the computations.

Given that the potential is a constant in the interior region, the wave equation (6.12) for $r < r_o$ is also of the form of (6.13) with k^2 replaced by $K^2 = k^2 + (2\mu V_o/\hbar^2)(1 + i\zeta)$, ζ being W_o/V_o. This means that the interior wave function is in general given by (6.14), and moreover we can discard the second term in (6.14) because n_ℓ is singular at the origin. Thus,

$$u_\ell(Kr) = A_\ell\, r j_\ell(Kr), \qquad r < r_o \tag{7.22}$$

with A_ℓ being some constant. Inserting this result into (6.24) we find the logarithmic derivative q_ℓ^{int} to be

$$q_\ell^{int} = 1 + Kr_o \frac{j'_\ell}{j_\ell} \tag{7.23}$$

The recurrence relation for q_ℓ^{int} follows from the property of the spherical Bessel function,

$$j'_\ell(z) = -\frac{\ell+1}{z} j_\ell(z) + j_{\ell-1}(z)$$

$$= \frac{\ell j_\ell(z)}{z} - j_{\ell+1}(z) \qquad (7.24)$$

Using (7.24) we can write (suppressing the superscript int)

$$q_\ell = -\ell + \frac{z j_{\ell-1}}{j_\ell} \qquad (7.25)$$

with $z = Kr_o$. Similarly, we have

$$q_{\ell-1} = 1 + (\ell+1) - \frac{z j_\ell}{j_{\ell-1}} \qquad (7.26)$$

Solving for $j_{\ell-1}/j_\ell$ in (7.26) and inserting the result into (7.25) we get

$$\boxed{q_\ell = \frac{z^2}{\ell - q_{\ell-1}} - \ell} \qquad (7.27)$$

This is the desired expression relating q_ℓ and $q_{\ell-1}$.

The relation (7.27) is also applicable to $q_\ell^{(\pm)}$ which are the logarithmic derivatives of essentially the exterior wave function (see (6.26) and (6.29)). We first write $q_\ell^{(\pm)} = \Delta_\ell \pm is_\ell$, thus defining the real and imaginary parts, and apply (7.27) by replacing q_ℓ by $\Delta_\ell \pm is_\ell$. Equating separately the real and imaginary parts on both sides, one gets

$$\Delta_\ell = \frac{\xi^2 (\ell - \Delta_{\ell-1})}{(\ell-\Delta_{\ell-1})^2 + s_{\ell-1}^2} - \ell \qquad (7.28)$$

$$s_\ell = \frac{\xi^2 s_{\ell-1}}{(\ell-\Delta_{\ell-1})^2 + s_{\ell-1}^2} \qquad (7.29)$$

with $\xi = kr_o$. Now (6.33) can be written as

$$\eta_\ell = e^{-2i\tau_\ell} \frac{q_\ell^{int} - \Delta_\ell + is_\ell}{q_\ell^{int} - \Delta_\ell - is_\ell} \tag{7.30}$$

with recurrence relations for $q_\ell^{(\pm)}$, Δ_ℓ, and s_ℓ, and for τ_ℓ one can use (6.32) directly.

To obtain the starting values at $\ell = 0$ we note that with $j_o(z) = \sin(z)/z$,

$$q_o(z) = z \cot(z) \tag{7.30}$$

One can show using (6.29) and (6.31) that

$$q_\ell^{(\pm)} = \xi \left[-\frac{1}{2v_\ell} \frac{dv_\ell}{d\xi} \pm i \frac{d\tau_\ell}{d\xi} \right] \tag{7.31}$$

Since $v_\ell^{-1} = \xi^2(n_\ell^2 + j_\ell^2)$, one finds that for $\ell = 0$, $v_o = 1$ and $\tau_o = \xi$.

Putting $q_o^{(+)} = \Delta_o + is_o$ in (7.30) we thus obtain

$$\Delta_o = 0, \qquad s_o = \xi \tag{7.32}$$

For actual computations it is useful to rewrite (7.30) once more to display the real and imaginary parts of q_ℓ^{int} explicitly,

$$\langle \eta_\ell \rangle = e^{-2i\tau_\ell} \left[1 - \frac{2s_\ell}{M_\ell + iN_\ell} \right] \tag{7.33}$$

with

$$M_\ell = s_\ell - \mathrm{Im} q_\ell^{int} \tag{7.34}$$

$$N_\ell = \mathrm{Re} q_\ell^{int} - \Delta_\ell \tag{7.35}$$

The compound formation cross section then becomes

$$\sigma_c = \sum_\ell \sigma_c^{(\ell)} \equiv \pi\lambda\!\!\!^{-2} \sum_\ell (2\ell+1)\, T_\ell(k) \tag{7.36}$$

where

$$T_\ell(k) = -4s_\ell \frac{\mathrm{Im} q_\ell^{int}}{M_\ell^2 + N_\ell^2} \tag{7.37}$$

The quantity $T_\ell(k)$, which is also equal to $1 - |\langle\eta_\ell\rangle|^2$, is called the transmission coefficient, and $\sigma_c^{(\ell)}/\pi r_o^2$ is sometimes known as the penetrability. In the same spirit, the total cross section becomes

$$\boxed{\sigma_t = 4\pi\lambda\!\!\!^{-2} \sum_\ell (2\ell+1) \left\{\sin^2\tau_\ell + s_\ell \frac{M_\ell \cos 2\tau_\ell - N_\ell \sin 2\tau_\ell}{M_\ell^2 + N_\ell^2}\right\} \equiv \sum_\ell \sigma_t^{(\ell)}} \tag{7.38}$$

Eqs.(7.36) and (7.38) are useful expressions for computing σ_c and σ_t, and then σ_{se} can be obtained by difference.

D. Numerical Results

We will quote some numerical results from problem set calculations of previous years to illustrate the kind of agreement with experiment one can obtain using the square-well model. The optical model values for fast neutron cross sections computed using the expressions derived above are shown in Table 7.1 along with experimental values taken from 'The Barn Book', BNL-325. Each calculated cross section is the sum of partial wave contributions from $\ell = 0$ to $\ell = \ell_{max}$. The most likely reason that σ_t is too low in the case of Al^{27} is that the higher order partial waves can not be ignored. In the other two cases σ_c is appreciably lower than the experimental data, whereas σ_t is seen to be within about 10%. The explanation is that the square well model, by virtue of the step change at the potential range r_o, gives rise to too much reflectivity at the surface of the nucleus, thus causing an underestimate of σ_c and correspondingly an overestimate of σ_{se}. This is an inherent feature of any discontinuous

Table 7.1 Neutron cross sections (barns) calculated using the square-well optical model and experimental data (in parenthesis)

nuclide	energy	ℓ_{max}	σ_t	σ_c	σ_{se}
Al^{27}	4.1 MeV	0	0.59 (2.4)	0.016	0.576
Bi^{209}	7	6	6.43 (5.86)	1.36 (2.5)	5.07 (3.36)
U^{238}	2	4	6.35 (7.0)	0.65 (2.5)	5.7 (4.5)

potential.

The most extensive comparison of square-well optical model calculations with experiment was reported in the paper of Feshbach, Porter, and Weisskopf. Fig. 7.1 shows the results for neutron cross section σ_t over the entire range of mass number and a range of energy, expressed in terms of $x^2 = [A^{5/3}/10(A+1)]E$, with E in MeV. The cross sections are given as $\sigma_t/\pi r_o^2$, where the potential range $r_o = 1.45 \times 10^{-13} A^{1/3}$ cm (shown as R in the figure). The other potential model parameter values are $V_o = 42$ MeV, and $\zeta = 0.03$. The experimental curves shown, taken from many sources, have been smoothed over since one is not concerned with the fine resonance structure in this comparison. Both calculations and

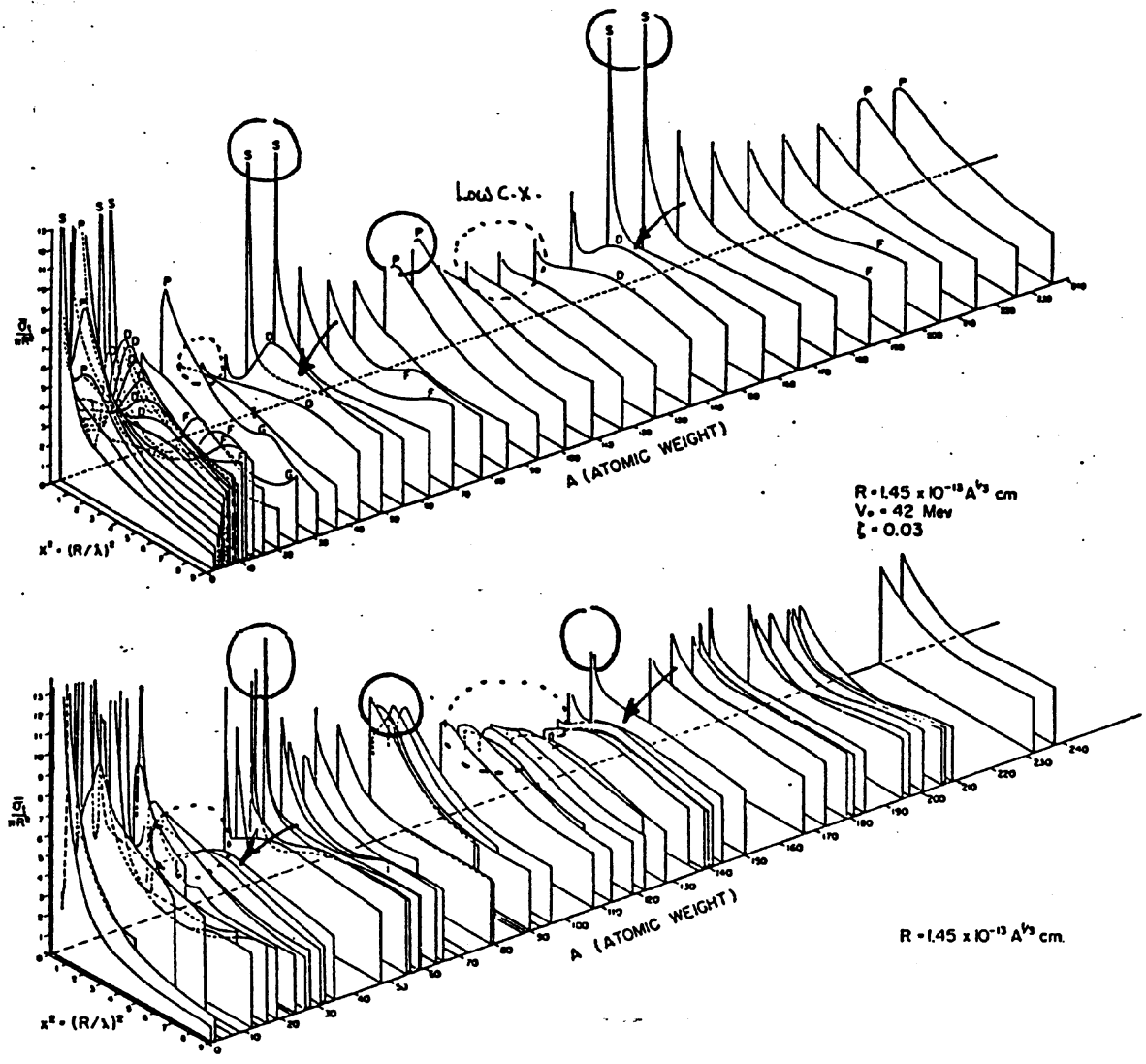

Fig. 7.1. Comparison of square-well optical model (upper) and observed (lower) neutron cross sections as a function of energy and mass number.

experimental data do not go below about 50 KeV.

It can be seen in Fig. 7.1 that the square-well optical model can account for a number of striking features (circled in the figure) of the experimental data. For example, there is a good correspondence in the low cross section values at low energy and around $A \simeq 40$ and $100 < A < 140$. Also the calculation shows the observed large cross sections at low energy and $A \simeq 60$ and 150 to be s-wave resonances and that at $A \simeq 90$ to be p-wave resonances. Furthermore, 'D maxima' can be seen for $x^2 \simeq 3$ and $A \simeq 40$ and 140.

An earlier comparison, using a smaller value of the potential well depth, $V_o = 19$ MeV instead of 42, did not give agreement as well as that shown in Fig. 7.1. It appears that the agreement is not sensitive to V_o so long as $r_o\sqrt{V_o}$ is kept constant. It is known that the shape of σ_t is quite sensitive to the value of ζ, the depth of the imaginary part of the potential. An increase in ζ tends to flatten out the maxima and minima, and using $\zeta = 0.02$ and 0.05 gives poorer agreement.

Comparison with experiment also has been carried out for the angular differential scattering cross section $\sigma_{el}(\theta)$. Fig. 7.2 shows two sets of calculations, one assuming that shape elastic scattering provides the only contribution, or $\sigma_{ce}(\theta) = 0$, and the other assuming a maximum contribution

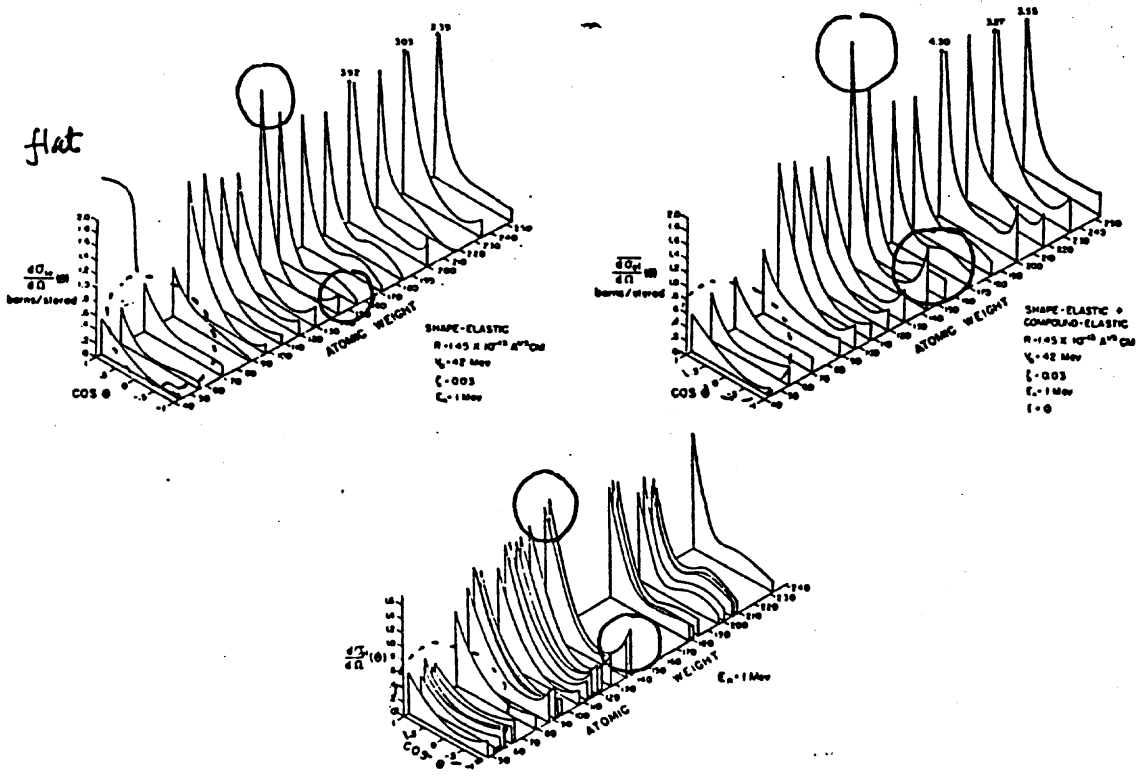

Fig. 7.2. Square-well optical model calculations (upper) and observed (lower) angular distribution of elastically scattered neutrons at 1 MeV.

from the compound elastic component, $\sigma_{ce} = \sigma_c$. These two assumptions correspond to the opposite extremes of underestimate and overestimate respecitvely. As in the comparison of σ_t a number of features in the experimental data are also seen in the optical model results, in particular the strong forward and backward scattering intensities at A ≃ 140, and a relatively flat distribution around A ≃ 60. Judging from the fact that the corresponding results for V_o = 19 MeV are not very different, one may conclude that $\sigma_{el}(\theta)$ is not sensitive to the potential well depth.

For further discussions of the square-well optical model one should see the original paper or Feshbach, Porter, and Weisskopf (1954).

E. Refinements of Square-Well Optical Model

There are several modifications of the square-well potential which give a more realistic description of the neutron-nucleus interaction. We will consider briefly such refinements and show a few results to illustrate the kind of improvements which one can expect to achieve.

Diffuse boundary effects

Since the square-well potential is known to give a value of σ_c that is too low, it is reasonable to use instead a continuous potential. A four-parameter form

$$V(r) = -(V_o + iW_o)\frac{1}{1 + e^{(r - R)/a}} \tag{7.39}$$

known as the Woods-Saxon potential has been adopted in a number of calculations. Here R is a measure of the nuclear radius and a is a measure of the boundary thickness. The main effect of the diffuse boundary is to lower the reflectivity at the surface, thus giving a larger value for σ_c.

Surface absorption

When the incident wave function starts to penetrate into the nucleus, one can imagine a self-shielding effect which results in more absorption taking place in the surface region as compared to the interior region. This would suggest that the imaginary part of the potential should be more concentrated in the surface region. One way to express this surface absorption behavior is to adopt the potential

$$V(r) = \begin{cases} -V_o & r \le R \\ -(V_o + iW_o \frac{d}{dx})\frac{1}{e^x - x} & r > R \end{cases} \tag{7.40}$$

with $x = (r - R)/a$.

Spin–orbit Coupling

All the discussions thus far have not taken into consideration that the interaction potential is in general spin–dependent. When the incident particle has a spin, such as neutron or proton, this angular momentum can couple with the orbital angular momentum of the particle and give rise to another contribution to the potential. If one wishes to include spin–orbit coupling in the calculation, one can write the potential as

$$V = V(r) + V_{so} \tag{7.41}$$

with

$$V_{so} = \text{cont.}\left[\frac{1}{r}\frac{dV(r)}{dr}\right] \underline{L}\cdot\underline{s} \tag{7.42}$$

Here V(r) is the central potential we have been discussing all along, $\underline{L}$ is orbital angular momentum operator of the incident particle, and $\underline{s}$ its intrinsic spin. The presence of spin–orbit coupling makes the potential V no longer spherically symmetric. Notice also that if the target nucleus has a nonzero spin I, then one can consider another contribution to V due to spin–spin coupling, the term being proportional to $\underline{s}\cdot\underline{I}$.

give ref.

There are numerical results which illustrate the importance of the optical model refinements we have just considered [Emmerich]. Fig. 7.3 shows that the use of diffuse boundary can indeed give a significantly improved agreement with experiment in the calculation of σ_c. The effects of surface absorption are not as large, but the evidence does point to an improvement over volume absorption. The effects of spin–orbit coupling seem to be important only in angular differential cross section at large scattering angles.

F. Nonlocal Optical Model

In determining the various parameters in an optical model one usually adopts those values which have been optimized by fitting to certain experimental data. It has been found that these parameters show considerable variation with energy. This is an unsatisfactory feature since the use of different sets of parameters for different energy ranges means that something fundamental is lacking in the model; also it gives less confidence in the predictive power of the model. To eliminate this feature one can formulate a nonlocal optical model as shown by Perey and Buck [Nuclear Physics 32, 353 (1962)]. It turns out that one can derive an energy–dependent relation between the nonlocal model and an equivalent local model, so a set of energy–independent parameters can be determined for the nonlocal model from which energy–dependent parameters for the local model can be obtained and the cross section calculation can proceed using the local model as discussed above.

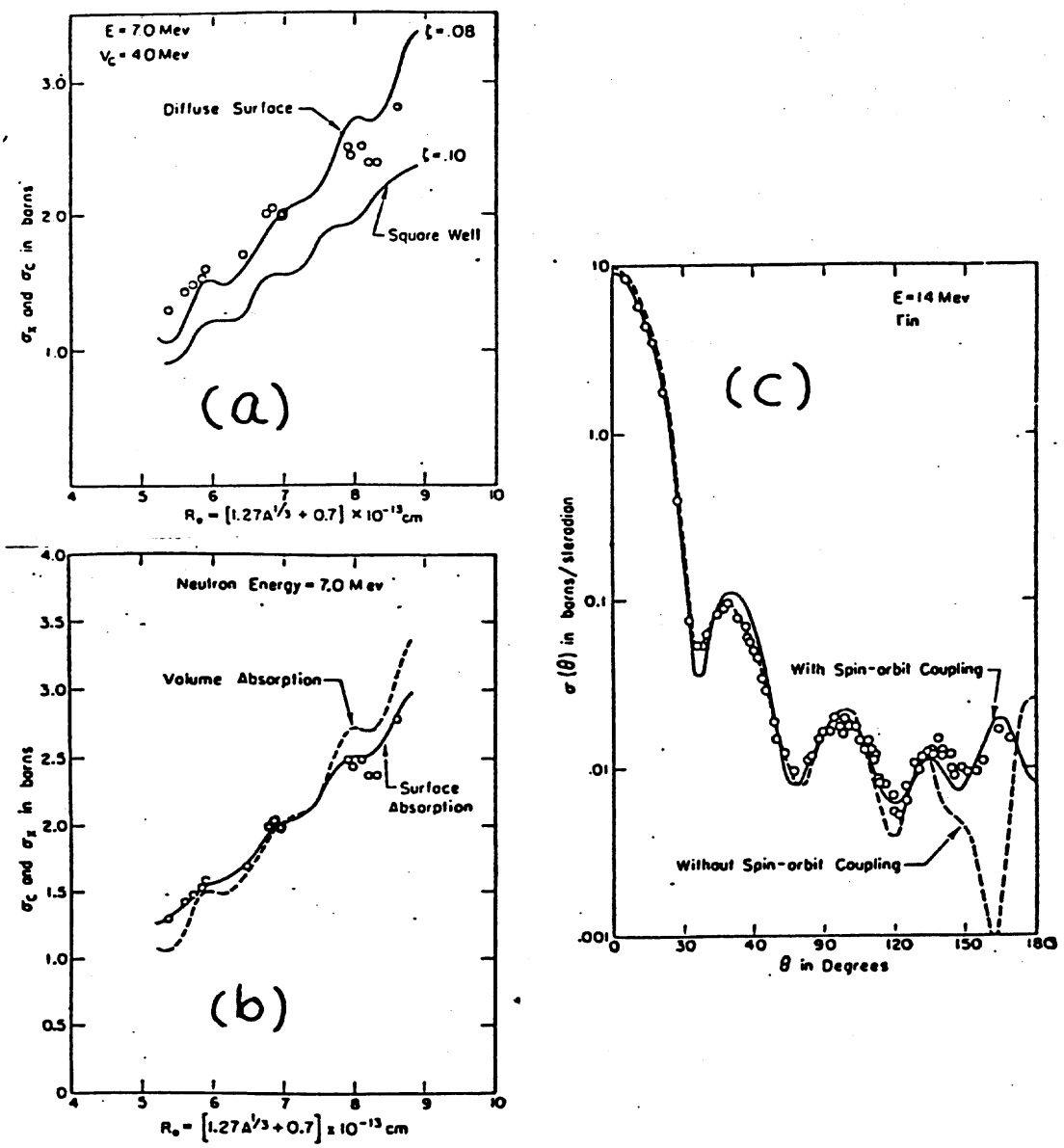

Fig. 7.3. Comparison of optical model calculations with experimental data showing the effects of diffuse boundary (a), surface absorption (b), and spin–orbit coupling (c).

We will give a brief discussion of the formulation of nonlocal optical model. One begins with the nonlocal wave equation

$$\frac{\hbar^2}{2\mu}\left[\frac{d^2}{dr^2} - \frac{\ell(\ell+1)}{r^2} + E\right] u_\ell(r) + \int_0^\infty dr'\, V(r,r')\, u_\ell(r') = 0 \qquad (7.43)$$

where $V(r,r')$ is related to the nonlocal potential $V(\underline{r},\underline{r}')$ according to

$$V(r,r') = 2\pi\, r\, r' \int_{-1}^{1} d\mu\, P_\ell(\mu)\, V(\underline{r},\underline{r}') \qquad (7.44)$$

For the form of $V(\underline{r},\underline{r}')$ one can choose two functions which depend on the

sum and difference of $\underline{r}$ and $\underline{r}'$,

$$V(\underline{r},\underline{r}') = U(\tfrac{1}{2}|\underline{r}+\underline{r}'|)\, H(|\underline{r}-\underline{r}'|) \tag{7.45}$$

with

$$-U(p) = V_o[1 + \exp\{(p-R)/a_s\}]^{-1} + iW_o 4e^{(p-R)/a_D}\,[1 + \exp\{(p-R)/a_D\}]^{-2} \tag{7.46}$$

$$H(|\underline{r}-\underline{r}'|) = [\pi^{3/2}\beta^3]^{-1} \exp\{-(r-r')^2/\beta^2\} \tag{7.47}$$

The function U(p) has the familiar form of a local optical model potential with diffuse boundary and surface absorption. The function H determines the form of nonlocality with β being a measure of the extent of nonlocal interactions. In the present model there are six parameters, V_o, W_o, a_s, a_D, R, and β. In addition one can add a spin–orbit coupling contribution.

One can derive an equivalent local potential given the particular form of the nonlocal potential model. Suppose we consider

$$[\frac{\hbar^2}{2\mu}\nabla^2 + E]\,\psi_N(\underline{r}) = \int d^3r'\, U_N(\tfrac{1}{2}(\underline{r}+\underline{r}'))\, H(|\underline{r}-\underline{r}'|)\psi_N(\underline{r}') \tag{7.48}$$

The right hand side of this equation can be written as

$$I = \int d^3s\, U_N(\underline{r}+\beta\underline{s}/2)\, [\pi^{3/2}\beta^3]^{-1}\, e^{-s^2}\, \psi_N(\underline{r}+\beta\underline{s}) \tag{7.49}$$

Notice that arguments of U_N and ψ_N can be shifted by the action of the gradient operator in the exponential form,

$$U_N(\underline{r}+\beta\underline{s}/2) = \exp(\beta\underline{s}\cdot\underline{\nabla}_1/2)\, U_N(\underline{r}) \tag{7.50}$$

$$\psi_N(\underline{r}+\beta\underline{s}) = \exp(\beta s\cdot\underline{\nabla}_2)\, \psi_N(\underline{r}) \tag{7.51}$$

where it is understood that $\underline{\nabla}_1$ acts only on $U_N(\underline{r})$ and $\underline{\nabla}_2$ only on $\psi_N(\underline{r})$. Then (7.49) becomes

$$I = [\int d^3s\, [\pi^{3/2}\beta^3]^{-1} \exp\{-\underline{s}\cdot\underline{s} + \beta\underline{s}\cdot(\underline{\nabla}_2 + \underline{\nabla}_1/2)\}]\, U_N(\underline{r})\, \psi_N(\underline{r}) \tag{7.52}$$

One can complete the square in the exponent and carry out the integration over s to obtain

$$I = \exp[\frac{\beta^2}{4}(\underline{\nabla}_2 + \underline{\nabla}_1/2)^2]\, U_N(\underline{r})\, \psi_N(\underline{r}) \tag{7.53}$$

If furthermore one assumes that the function $U_N(\underline{r})$ is sufficiently slowly varying that the effect of the operator $\underline{\nabla}_1$ can be ignored, then (7.48) becomes approximately

$$[\frac{\hbar^2}{2\mu} \nabla^2 + E] \psi_N(\underline{r}) \simeq U_N(\underline{r}) \exp(\beta^2\nabla^2/4) \psi_N(\underline{r}) \tag{7.54}$$

We can compare (7.54) with the usual local optical model equation

$$[\frac{\hbar^2}{2\mu} \nabla^2 + E] \psi_L(\underline{r}) = U_L(\underline{r}) \psi_L(\underline{r}) \tag{7.55}$$

We define an equivalent local potential by requiring that the cross section calculated from (7.54) and (7.55) be the same. Since this will be the case if the two wave functions $\psi_N(\underline{r})$ and $\psi_L(\underline{r})$ are the same, we have from (7.55)

$$\frac{\hbar^2}{2\mu} \nabla^2 \psi_N(\underline{r}) = - [E - U_L(\underline{r})] \psi_N(\underline{r}) \tag{7.56}$$

so that (7.54) gives

$$U_L(\underline{r}) \psi_N(\underline{r}) \simeq U_N(\underline{r}) \exp\{ - \frac{\mu\beta^2}{2\hbar^2} [E - U_L(\underline{r})]\} \psi_N(\underline{r}) \tag{7.57}$$

or

$$U_L(\underline{r}) \exp\{ \frac{\mu\beta^2}{2\hbar^2} [E - U_L(\underline{r})]\} = U_N(\underline{r}) \tag{7.58}$$

This is the desired relation which one can use to derive an equivalent local optical model potential $U_L(\underline{r})$ that is energy dependent from a nonlocal optical model $U_N(\underline{r})$.

Two methods have been proposed to obtain $U_L(\underline{r})$ from the nonlinear relation (7.58), an iterative procedure [Wilmore and Hodgson, Nuclear Physics 55, 673 (1964)] and an approximate analytical procedure [Gersten, Nuclear Physics A 96, 288 (1967)].

The nonlocal optical model potential used by Perey and Buck was optimized by fitting the neutron cross sections of lead in the energy range 7 to 14.5 Mev. The parameters values found are

$V_o = 71$ MeV $a_s = 0.65 \times 10^{-13}$ cm

$W_o = 15$ $a_D = 0.47$

$U_{so} = 1300$ $R = 1.22\ A^{1/3}$

and $\beta = 0.85$.

Table 7.2 shows a comparison of some results of the nonlocal optical model and the equivalent local potential calculations with experiment.

Table 7.2 Comparison of total neutron cross sections σ_t (in barns) with deviation from experiment shown in parenthesis.

nuclei	E [MeV]	nonlocal	eq. local	BNL-325
Si^{28}	5.95	2.33 (+11%)	2.24 (+7%)	2.1
Sc^{45}	1	3.52 (+17%)	3.38 (+13%)	3
Fe^{56}	3.26	3.85 (+10%)	3.71 (+6%)	3.5
W^{184}	1.37	6.44 (-8%)	6.27 (-10%)	7
Bi^{209}	7	6.21 (+6%)	6.03 (+3%)	5.86

One can see from Table 7.2 that the nonlocal potential cross sections are generally higher than measurements by about 10% and that they are consistently higher than the equivalent local potential results by 3-5%. The same behavior also holds for the two contributions to σ_t, namely, σ_{se} and σ_c. From studies such as these one may conclude that the equivalent local potential model combines the advantages of an energy-independent nonlocal potential with the relative simplicity of a local potential calculation.

Perhaps the most comprehensive test of the nonlocal optical model formulation is shown in Fig. 7.4, where the calculated neutron cross sections σ_t and σ_c are compared with experimental data at 4.1, 7, 14.5, and 24 MeV over the entire range of mass numbers. This is definitive evidence that the nonlocal potential model is capable of predicting fast neutron cross sections for most nuclei up to 30 MeV to within 10% or better. It is interesting to note that the results of Perey and Buck are as good as the most successful attempt to fit neutron data in the energy range 4.1 - 14.5 MeV with a local potential with energy-dependent potential parameters [see Bjorklund and Fernbach, Phys. Rev. 109, 1295 (1958)].

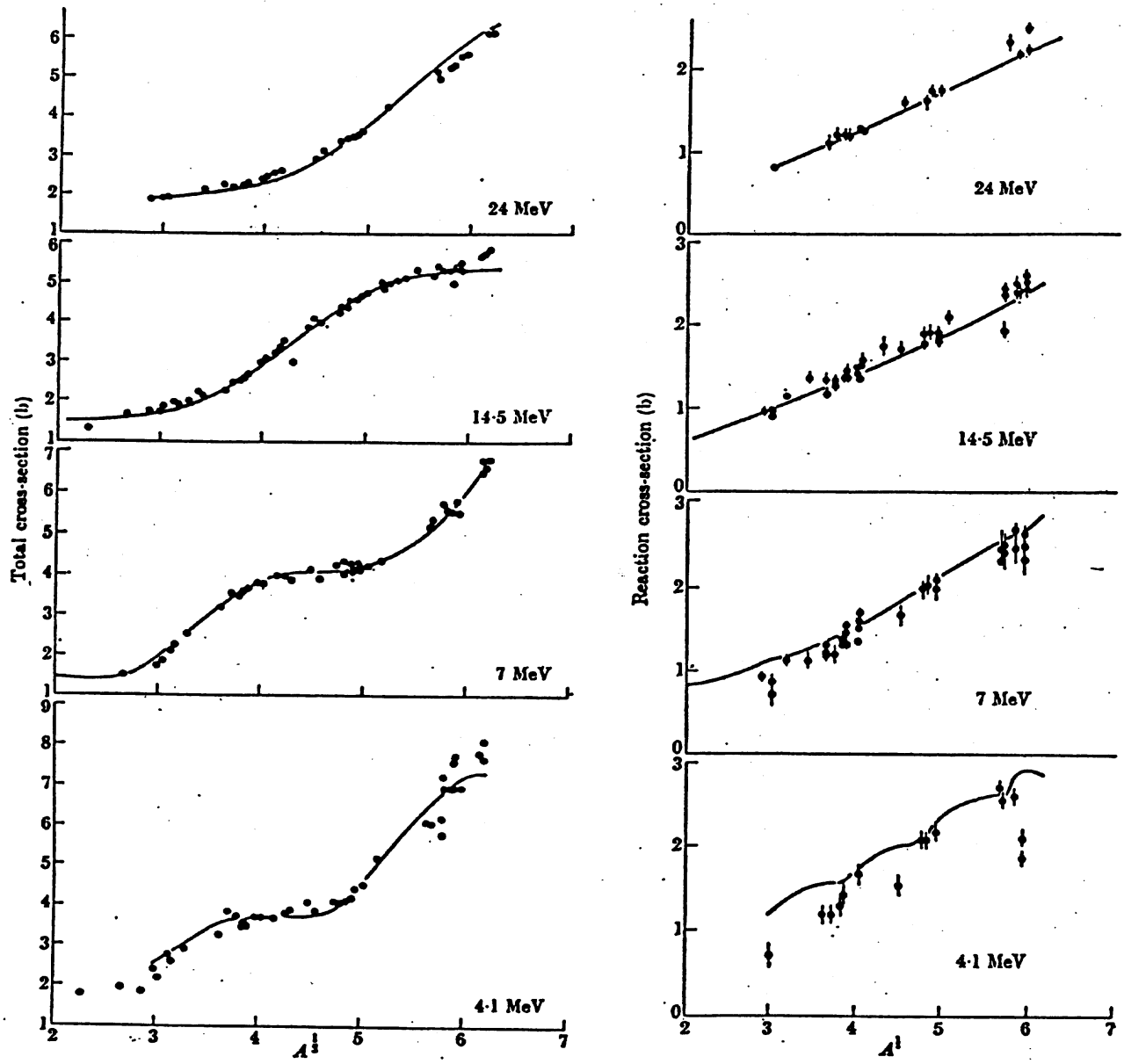

Fig. 7.4. Comparison of nonlocal optical model calculations [Perey and Buck] of neutron cross sections with experimental data.

As a final comparison with experiment we show in Fig. 7.5 the effective potential scattering radius derived from the low-energy limit of σ_{se},

$$4\pi a^2 = \sigma_{se}(E)\big|_{E\to 0} = \lim_{k \to 0} [\pi\lambda\!\!\!^{-2} |1 - \langle\eta_o\rangle|^2] \qquad (7.59)$$

where $\langle\eta_o\rangle$ is the s-wave scattering matrix calculated using the optical model. The quantity a is known as the scattering length; it is of

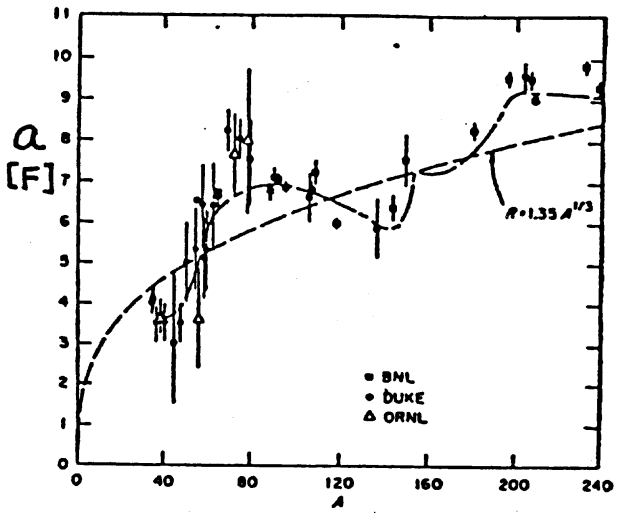

Fig. 7.5. Comparison of optical model calculation of scattering radius a with experiment.

considerable interest in the study of thermal neutron scattering as we will see in Chap. IX. Also shown in Fig. 7.5 is the simple approximation of taking the scattering radius to be proportional to the size of the nucleus. One sees that there is definite structure in the variation of a with atomic weight, although the general trend follows more or less the $A^{1/3}$ behavior, and optical model is able to give quite accurate predictions of the scattering cross section at low energy across the entire range of A.